DISTRIBUTED TEMPERATURES IN THE SNOW ZONE: SPATIAL PATTERNS AND INNOVATIVE MEASUREMENT TECHNIQUES

Jessica D. Lundquist[1] and Caitlin Rochford[2]

ABSTRACT

Mountains are spatially complex and sparsely sampled. Temperatures are usually interpolated from distant stations assuming a standard atmospheric lapse rate (decrease of 6.5°C per 1000 m elevation gain). However, examination of observed surface temperatures indicates that temperature patterns differ diurnally, synoptically, and seasonally and do not always increase linearly with elevation. This can have profound impacts on snowmelt and runoff forecasts. Fortunately, new technology has become available to monitor temperature in remote locations, such as the Onset Hobo and the Maxim i-button. Approximately 200 of these self-recording sensors have been deployed in Yosemite National Park, California and Niwot Ridge and Rocky Mountain National Park, Colorado over the past several years. Empirical orthogonal functions (EOFs) are used to identify the dominant spatial temperature patterns within each study area and how they vary in time. The spatial patterns of temperature are correlated with topography, such as windward-slope, lee-slope, valley, or ridge. Temporal variations of these surface temperature patterns are correlated with large-scale weather conditions, such winds and pressure patterns. Comparison between study sites allows for generalizations of temperature patterns across space (mapping spatial patterns using topography) and time (mapping temporal variations using large-scale weather parameters), which can be utilized in more sparsely sampled areas. Experimentation with such a large number of sensors also illuminates how to best deploy these small instruments to sample topographically-controlled, versus vegetation-controlled, versus radiation-controlled, temperatures.

INTRODUCTION

In the western United States, over half of the water supply is derived from mountain snowmelt, where the snow delays runoff and provides water in the spring and summer, when it is needed most. In recent decades, snowmelt runoff timing has advanced one to three weeks earlier in mountainous catchments across western North America, responding primarily to temperature changes (Hamlet et al. 2005; Stewart et al. 2005). However, these general trends are quite variable between basins, and at high elevations, little is known about the spatial and temporal variations of critical processes like snowmelt, runoff, or even temperature.

Mountains are spatially complex and sparsely sampled. Temperatures are usually interpolated from distant stations assuming a decrease in air temperature of 6.5°C per 1000 m elevation gain, which is the standard atmospheric lapse rate. However, examination of observed surface temperatures indicates that they differ diurnally, synoptically, and seasonally and do not always increase linearly with elevation, which can have profound impacts on snowmelt and runoff forecasts. For example, Singh (1991) found that changes of 1°C per km in the lapse rate for the Beas watershed (345 km^2, spanning 1900 to 5400 m elevation) produced variations of 28-37% in the modeled snowmelt runoff over a two-month period.

Fortunately, new technology has become available to monitor temperature in remote locations (Lundquist et al., 2003), such as Onset Tidbits, Pendants, and Hobos (http://www.onsetcomp.com), and Maxim i-buttons (http://www.maxim-ic.com/products/ibutton/). These instruments, and new competitors on the market, are inexpensive (about $30 each at the time of this presentation) and can be densely deployed across mountain landscapes. Temperature variations across a landscape are controlled primarily by local topography, vegetation, and larger-scale weather patterns. Thus, if the relationships between these patterns, local temperature, and standard atmospheric measurements can be established over a short time period (e.g., a year), we can use these relationships

Paper presented Western Snow Conference 2007
[1] Assistant Professor, Civil and Environmental Engineering, University of Washington, Box 352700, Seattle, WA 98195-2700, jdlund@u.washington.edu
[2] NOAA Hollings Scholar, Saint Louis University, rochford@slu.edu

to better interpret how representative temperatures at long-term stations are of temperatures in the surrounding environment, to better interpolate temperature across the landscape, and to improve models of snowmelt and runoff. This paper describes spatial temperature variations observed by distributed sensors in Yosemite National Park (2001-2005) and in Rocky Mountain National Park (2005-2006) and how they relate to large-scale weather patterns. A method for identifying regions of likely cold-air drainage is described. Finally, deployment techniques, such as putting i-buttons with the evergreen forest canopy to shield them from solar radiation, are discussed.

YOSEMITE, CALIFORNIA INTENSIVE STUDY AREA: PATTERNS OF TEMPERATURE AND EMPIRICAL ORTHOGONAL FUNCTIONS

Instruments and Deployment Techniques

Over 60 temperature sensors have been deployed in and around Yosemite National Park since summer 2001, primarily along the Tioga Road and the river corridors of the Tuolumne and Merced (Lundquist et al., 2003). The Tioga Road (California Route 120) is the highest road passing over the Sierra Nevada, and traverses the west slope of the Sierra Nevada through Yosemite National Park and the east slope through Lee Vining Canyon and down into the Owens Valley. Sensors across this transect included small, inexpensive, self-recording temperature sensors, which sampled at hourly intervals and whose data were manually retrieved and downloaded each year, and more traditional temperature sensors, such as snow pillows, co-op stations, and RAWS stations, which provided telemetered, real-time hourly or daily maximum and minimum temperature data (Figure 1). The sensors are collectively referred to as the Yosemite network.

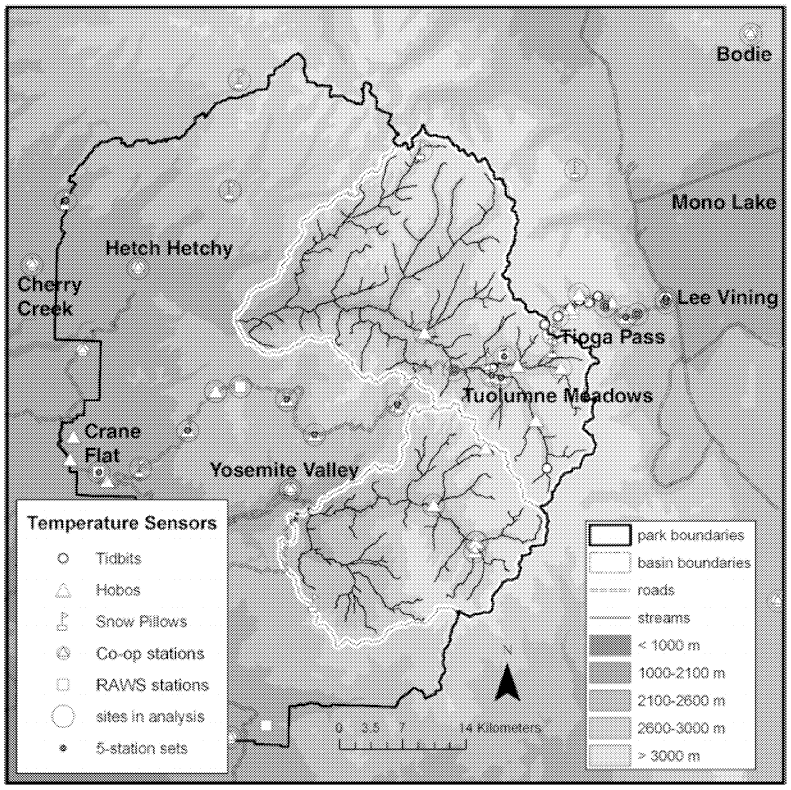

Figure 1. Map of Yosemite network sensors in the central Sierra Nevada of California. Elevation zones correspond to different vegetation zones: lower montane (~1000-2100 m), upper montane (~2100-2600 m), and subalpine (~2600-3000 m) forests on the west slope, and between upper montane (~3000-2600m), lower montane (~2600m-2100m), and piñon pine, juniper and aspen (<2100m) forests on the east slope. Circled sites had sufficient data to be included in the analysis, and stations with black dots were included in regional averages (e.g., Figure 4).

As a description of average conditions, i.e., two-year-mean temperatures at the 37 stations with substantial data from July 2002 to July 2004, a linear lapse rate is a reasonable model of the temperature structure in the Yosemite network. The RMS errors between the data and lines based on both a linear fit to the data (slope of -6.8°C km^{-1}) and the standard lapse rate (slope of -6.5°C km^{-1}) are 1.1°C. However, the daily data (Figure 2) reveal that temperatures only sometimes decrease linearly with elevation. On 1 to 3 January 2004, the weather in the

Yosemite region was dominated by a low-pressure system with strong westerly winds. Temperatures decreased linearly with elevation and matched closely with free-air temperatures observed by the Oakland sounding (Figure 2a-2c). However, by 4 January 2004, the low-pressure system migrated eastward, and high pressure developed over the study area. Wind speeds greatly decreased. Clear skies and frigid temperatures (daily means ranging from -8 to -24°C) resulted in cold-air drainage to the meadows and valleys, and mean daily temperatures at many Yosemite sites were over 15°C cooler than those measured at equivalent elevations at Oakland (Figure 2d). The flattest locations, particularly those in the bottom of broad, U-shaped valleys, such as the Tuolumne Meadows area stations in the Yosemite network, became the coldest, so that temperatures increased with elevation above these areas. Temperatures continued to be uncorrelated with elevation over the next two days (Figure 2e-2f), suggesting that topographic characteristics other than elevation were exerting strong controls on temperatures across the landscape. This example illustrates the need to determine how patterns vary spatially, rather than focusing specifically on temperature changes with elevation.

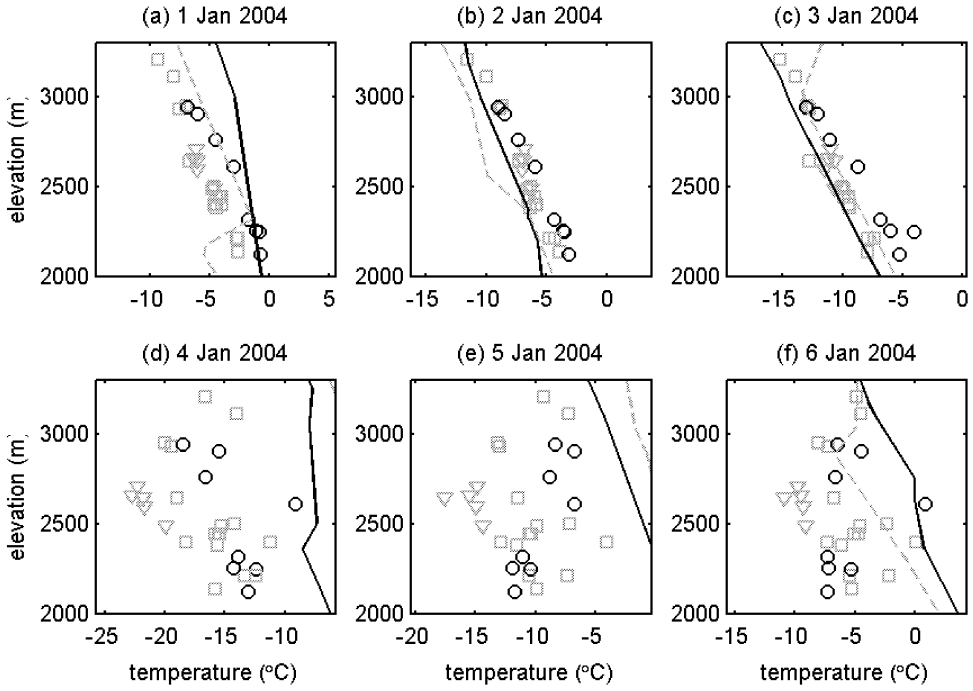

Figure 2. Temperature vs. elevation for six days in January 2004. Gray dashed line is morning (0400 PST) sounding at Oakland; black solid line is afternoon (1600 PST) sounding at Oakland. Black circles are average daily temperatures at east slope stations; gray symbols are west slope stations, where triangles represent stations in the Tuolumne Meadows region, and squares represent stations along the Tioga Road. Note: In 2d, the dashed line is off the scale because the morning sounding was even warmer than the afternoon sounding (from Lundquist and Cayan, 2007).

Spatial Patterns of Temperature Variation (EOFs)

Empirical orthogonal functions (EOFs) can be constructed using singular value decomposition [SVD, Anderson et al., 1999] to decompose a dataset into its principal spatial patterns of variation and their evolution through time (Preisendorfer, 1988). The EOFs are linear and orthogonal, such that a sum of each spatial component multiplied by its corresponding temporal variation recreates the original temperature dataset, and are normalized, such that the variances of all components sum to one. Because the Yosemite network domain is smaller than that of synoptic weather systems, the predominant spatial pattern of the raw data is that all locations vary together (i.e., if one site is warmer, all are warmer), where each site has a weight proportional to its mean temperature for the analysis period. The corresponding temporal evolution (here referred to as the principal component, PC) of this pattern represents spatially-averaged temperature fluctuations over the region.

In this study, we are interested in how sites within the Yosemite network differ from regional estimates of temperature (represented here by the NCEP-NCAR Reanalysis data, Kalnay et al. 1996) and from each other over time. Thus, we set up the analysis to focus on spatial variations from the regional mean. With this in mind, the

700-hPa temperature residuals (T_{700}'), representing the regional average temperature fluctuations, were considered a "known" baseline and were removed from the surface temperature residuals (T_{surf}'). Thus, the resulting surface temperature anomalies can be considered as departures from 700-hPa free air temperature anomalies ($T_{var}' = T_{surf}' - T_{700}'$).

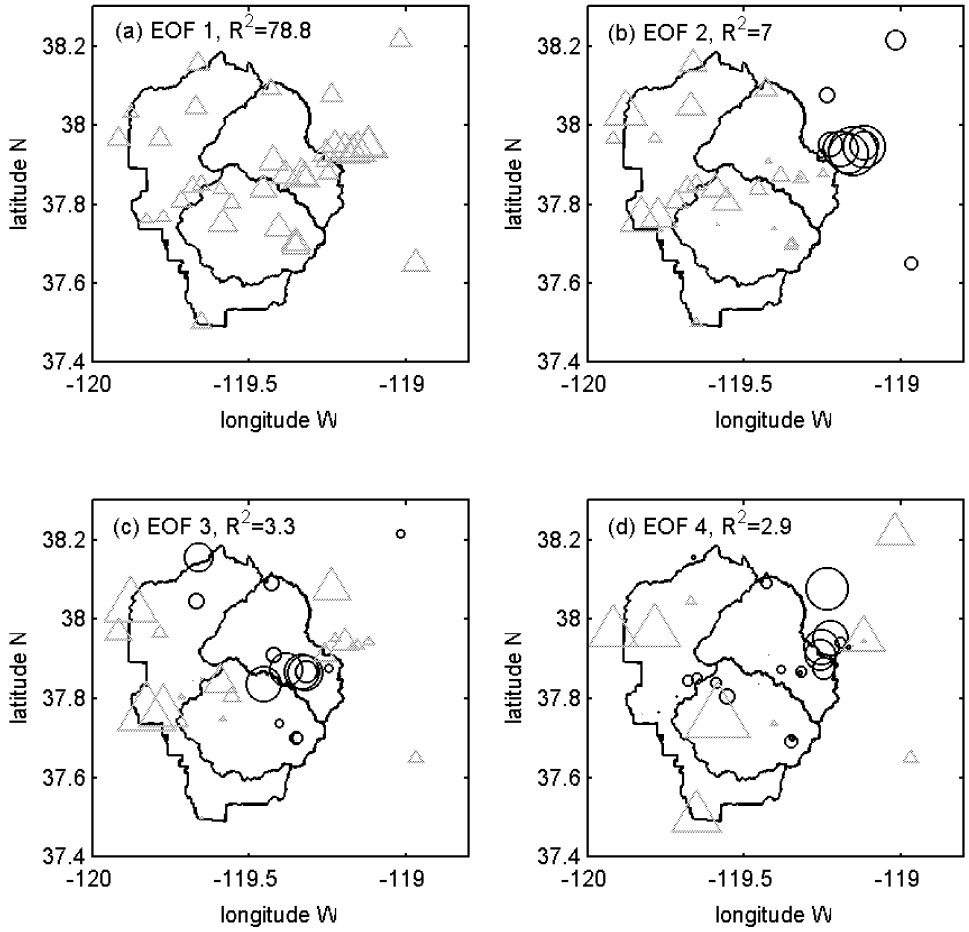

Figure 3. First four spatial EOFs for Yosemite temperatures: Gray triangles indicate positive; black circles indicate negative weights, and the size of the symbol indicates the magnitude of the weight for each station. Black outlines represent the park boundaries and the Tuolumne and Merced watersheds, thus defining the ridgelines (highest towards the northeast) within the area (from Lundquist and Cayan 2007).

The first few EOFs represent the primary modes of variability of the residual temperature patterns across the Yosemite landscape (Figure 3). The first mode (EOF 1, 78.8% of the variance) is representative of a pattern having roughly uniform temperature deviations, of the same sign (all positive or all negative) over all of the stations in the Yosemite network (Figure 3a). The second mode (EOF 2, 7.0% of the variance, Figure 4b) represents differences in surface temperature deviations between the west slope and the east slope of the Sierra. The second mode (EOF 2) is correlated with the wind direction across the Sierra Nevada (R = -0.46 with zonal winds, Table 3). The third mode (EOF 3, 3.3% of the variance, Figure 3c) identifies areas that are well drained, in contrast to those that are prone to accumulation of cold-air, such as the Tuolumne Meadows region of Yosemite National Park (Figure 1, large circles in Figure 3c). These are the areas that were exceptionally cold during the 4-6 January 2004 case study. Occurrences of positive PC 3 were strongest when positive geopotential height anomalies, i.e., anomalously high pressure and anomalously low humidity air masses, were seated over the western U.S. the previous day, evidenced by correlations with prior day 700-hPa geopotential height (R=0.49) and with the prior day relative humidity (R = -0.51). This is consistent with prior results, which have shown that cold-air drainage occurs most prominently in dry-air, clear-sky conditions with weak synoptic activity (Barr and Orgill, 1989; Anquetin et al., 1998) and is more pronounced downslope of converging canyons, which feed cold air into a downslope valley (Neff and King, 1989),

such as the flat, wide, U-shaped valley of Tuolumne Meadows. Figure 4 illustrates the average diurnal temperatures for groups of stations on the west slope, east slope, and in Tuolumne Meadows (dots in Figure 1) for days with high (Figure 4a) and low (Figure 4b) values of PC 3. The fourth mode (EOF 4, 2.9% of the variance, Figure 3d) correlates well with elevation. Positive values represent a strengthening, and negative values represent a weakening of the temperature lapse rate.

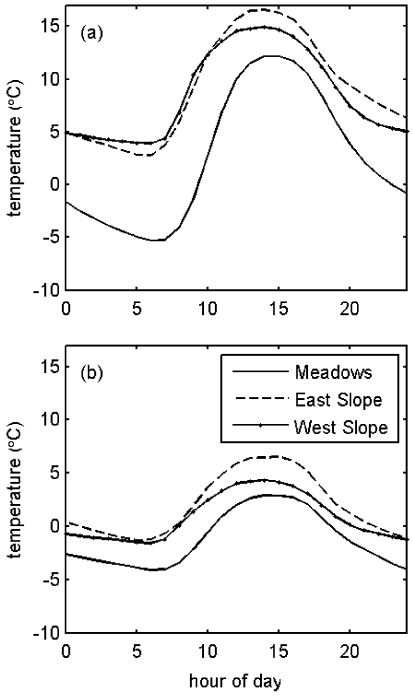

Figure 4. Average hourly temperatures (°C) in PST at representative stations on days with (a) PC 3 values > 1 standard deviation above average and (b) PC 3 values < 1 standard deviation below average. Notice the much greater differences in minimum temperatures and diurnal range between the 3 different regions during days with high PC 3 (from Lundquist and Cayan, 2007).

ROCKY MOUNTAIN NATIONAL PARK STUDY: GENERALIZING SPATIAL PATTERNS OF COLD-AIR DRAINAGE

I-button temperature sensors were densely deployed in a variety of elevations, aspects, and vegetation types in the the long-term ecological research (LTER) station at Niwot Ridge, on the east side of the continental divide, which has 4 climate stations that have been operational since 1952, the Loch Vale Watershed of Rocky Mountain National Park (RMNP), which has 3 weather stations operational since 1991, to test the following: 1) What are the pros and cons of using inexpensive temperature sensors? 2) How well do long-term meteorological stations represent the surrounding topography? 3) What roles do temperature inversions and cold-air ponding play in spatial temperature variations? 4) How do localized temperature patterns relate to large-scale weather patterns, such as pressure, wind speed and direction, or cloudiness? Instruments were suspended from tree branches below treeline and attached to rebar and PVC pipe above treeline, using upside-down funnels for radiation shields. Each site was documented with GPS measurements and photographs.

EOF analysis similar to that carried out for Yosemite National Park (previous section, Lundquist and Cayan, 2007) showed that the dominant mode of variation for Niwot Ridge is a strengthening/weakening of the lapse rate (similar to Yosemite EOF 4) and for Rocky Mountain National Park (RMNP) is cold-air drainage near the Loch (similar to Yosemite EOF 3). Both of these spatial patterns were strongly correlated with large-scale winds, which are normally fast and from the west. When the wind speeds drop, local topography becomes more important, and local patterns of cold-air drainage can develop. High-density distributed temperature sensors can easily identify where on the landscape cold-air drainage is important (Lundquist and Cayan, 2007), but these locations need to be related to the characteristics of a digital elevation model (DEM) so that cold-air drainage can be modeled over areas

where such high-resolution temperature data are not available. Any distributed snowmelt model requires a map of distributed temperature across a basin, and errors in interpolating temperature correctly across complex terrain are one of the largest sources of error in distributed modeling (Liston and Elder, 2006). These errors are particularly large in areas subject to cold-air drainage, where even high-resolution atmospheric models are often biased 3 to 4°C during cold-pool events (Hart et al., 2005).

Because the dominant spatial patterns of temperature variation are similar between the study sites in California and Colorado, we identified topographic characteristics from their DEMs that can be used to generalize the geographic locations of the spatial patterns of variation. For example, an index of valley bottom flatness for mapping depositional areas, based on slope and the rank of elevation with respect to the surrounding area (Gallant and Dowling 2003) provides an automated method to determine regions of likely cold-air drainage. This can be tested in areas with distributed temperature measurements, such as the Loch Vale Watershed in Colorado (Figure 5). Most of the sites identified as locations with or without cold-air drainage agree with the DEM-based classification, with the exception of the eastern-most site at the mouth of the Loch, where a sill blocks cold air from draining further down the valley. Cold-air drainage is correlated with large-scale patterns of weak winds and high pressure, and these large-scale weather patterns can be used to predict when cold-air drainage is an important part of the spatial temperature distribution (Lundquist and Cayan, 2007). While this work is preliminary, it can provide a geographic mapping of where on the landscape nighttime temperatures should be lowered during periods of weak winds and high pressure.

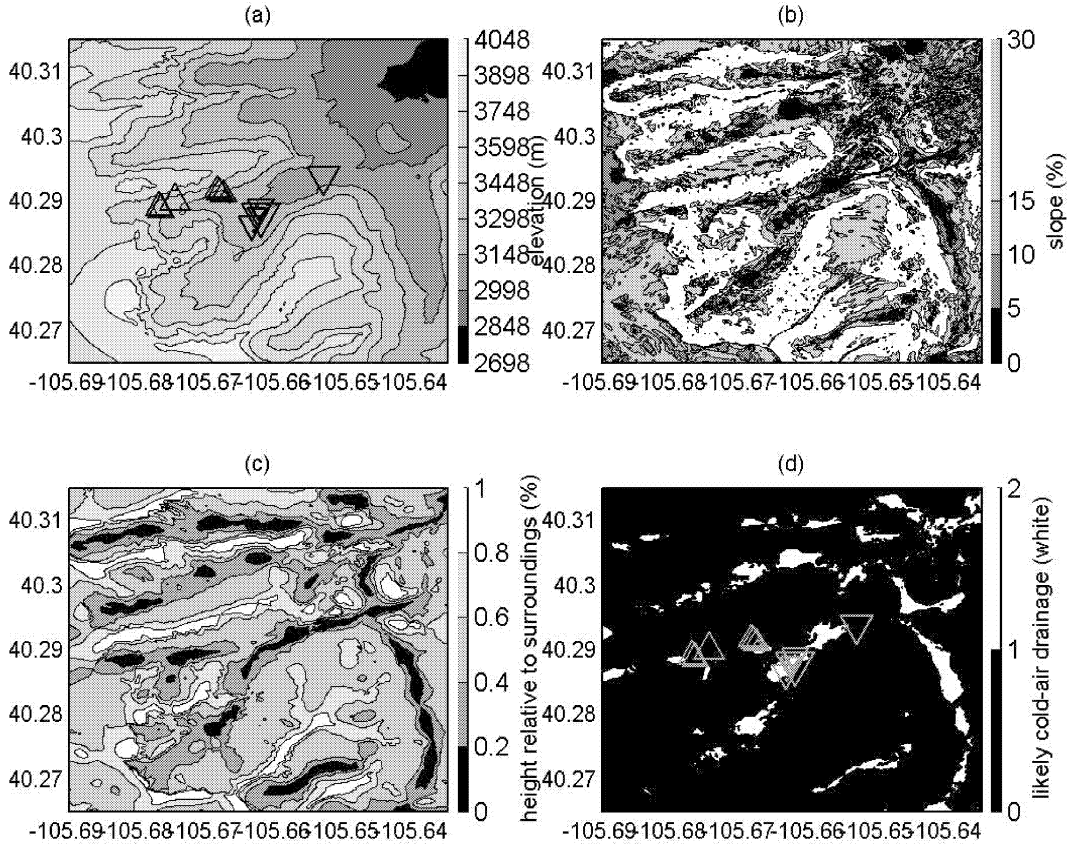

Figure 5. Maps of (a) elevation, (b) slope, (c) percentile of elevation to surrounding elevations, and (d) selected areas of likely cold-air drainage across the landscape, based on criteria of slope < 15% and percentile < 40%, for Loch Vale watershed in Rocky Mountain National Park, Colorado. Downward-pointing triangles indicate monitored locations that are sensitive to cold-air drainage, and upward-pointing triangles indicate areas that do not experience cold-air drainage.

I-BUTTONS: DEPLOYMNET TECHNIQUES, TREES, AND SOLAR RADIATION

The Maxim I-button Sensor

Hubbart et al. (2005) tested 31 thermochron i-buttons and found them to be accurate within ± 0.21 °C (even better than the manufacturer listed accuracy of ± 1 °C. For this study, we examined over 100 Dallas Semiconductor Maxim iButtons (DS-1922L). These are listed as having an accuracy of ±0·5 °C but tested as accurate to ±0·2 °C when submerged in an ice bath. These instruments are 17.35 mm in diameter, 5.89 mm thick, and have a temperature range of -35 °C to +85 °C. The user defines a sampling interval from 1 s to 273 hr, and instruments can record 8192 8-bit readings at 0.5 °C resolution or 4096 16-bit readings at 0.0625 °C resolution. We programmed the instruments to sample once per hour at 0.5 °C resolution, which allowed them to collect 11 months of data. The instruments can be programmed to stop recording at this point or to record over the earliest data.

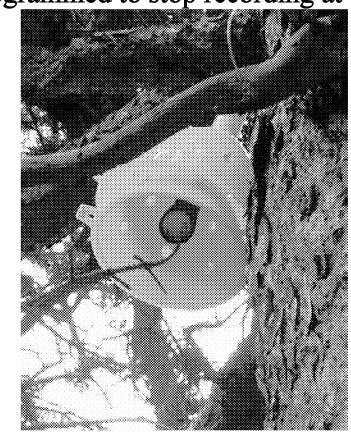

Figure 6. Photo of i-button sensor in upside-down funnel radiation shield in a pine tree

Sensor Performance: Deployment Strategies

Between August 2005 and July 2006, approximately 100 i-buttons were deployed on the eastern slopes of the Colorado Rocky Mountains. 100% of these were retrieved and still functioning at the end of the study period. Sensors that were properly shielded from solar radiation, i.e., in a Stevenson Screen, reported temperatures that closely matched those recorded by standard instruments (RMSE = 1.0°C and R^2 = 0.99). I-button temperatures were on average 0.4°C cooler than the daily maximum and 0.4°C warmer than the daily minimum, but this is within the range of accuracy specified by the manufacturer.

Most i-buttons were deployed with an upside-down funnel shield developed by Jason Hubbart (personal communication, 2005), which shielded them from solar radiation from above but not reflected solar radiation from below (Figure 6). This resulted in large errors for sensors hung from poles (Bias = 3.9°C, RMSE = 5.3°C, and R^2 = 0.81), with the largest errors occurring on sunny days when snow was on the ground. Fortunately, most sensors were deployed deep within pine trees, which provided radiative shielding from both above and below (Bias = 0.1°C, RMSE = 1.0°C, and R^2 = 0.98), comparable to the statistics for sensors co-located within a Stevenson Screen. A sensor within an Aspen tree received much more solar radiation in the winter, reflected from the snow. A sensor in a krumholtz at treeline was covered with snow most of the winter, recording a well-insulated 0 °C. Thus, if one's objective is to measure atmospheric temperature, it is important to deploy sensors in evergreen trees, high enough to remain above the accumulated snowpack, whenever possible.

Tuolumne Meadows Tree Experiment

To further compare the effects of deployment within trees on temperature, three i-buttons were installed next to a standard meteorological and snow pillow station in Tuolumne Meadows, Yosemite, California: one on a pole, one in a solitary Lodgepole pine, and one within a dense stand of Lodgepole pines. The temperature sensor in the dense stand of trees most closely reproduced the temperature reported by the standard temperature sensor on the meteorological tower.

The difference between the temperature measured by the sensor on the pole, which lacked radiative shielding from below, and the temperature measured by the sensor within the dense stand of trees correlated well with independent measurements of solar radiation (R^2=0.78, Figure 7a). This correlation was significantly higher than the correlation of radiation with the diurnal temperature range, T_{max}-T_{min} (R^2=0.23, Figure 7b), which is often used as a proxy for solar radiation when direct measurements are not available. The temperature difference also closely tracks changes in surface albedo, with the daytime temperature difference nearly doubling when snow is on the

ground. Thus, pairs of differently shielded temperature sensors could provide a cheap proxy for distributed cloud cover (ie., solar radiation) and albedo changes.

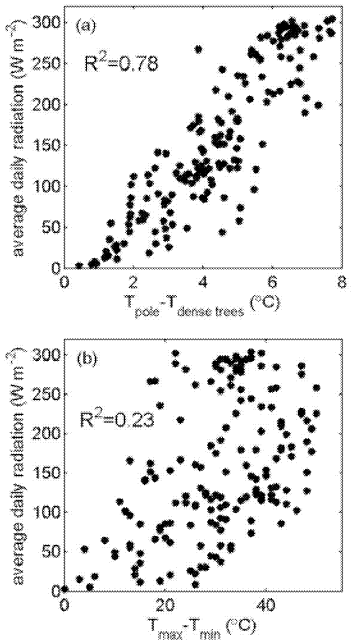

Figure 7. Correlation of temperature differences with solar radiation

SUMMARY, DISCUSSION, AND CONCLUSIONS

Temperatures in complex terrain are poorly sampled, and measurements and standard lapse rates may not represent the temperatures of the surrounding topography. Rather, temperature patterns are strongly influenced by large-scale weather patterns and how regional winds and cold-air drainage interact with existing topography. Small new self-recording temperature sensors make distributed measurements possible, and short-term intensive sampling, combined with EOF analysis, can help identify the spatial and temporal patterns of regional temperature variations. Likely locations of spatial differences can be identified by analyzing basin DEMs, and temporal fluctuations can be correlated with large-scale weather parameters (such as wind speed, wind direction, and 700 hPa geopotential height). Evergreen trees provide a practical, inexpensive way to shield sensors from solar radiation and to keep sensors above winter snowfall. Together, these techniques can improve how we model temperature variations across complex terrain.

ACKNOWLEDGEMENTS

Brian Huggett (NPS), Dan Cayan (SIO), Mike Dettinger (USGS), Heidi Roop (Mt. Holyoke), Jim Roche (NPS), Frank Gehrke (CA DWR), Kelly Redmond (WRCC), Canon Research Fellowship, NSF RoadNET program, CIRES Postdoctoral Fellowship., CIRES Innovative Research Fellowship, Dave Clow (Colorado USGS), Mark Losleben (Colorado Mountain Research Station(MRS)), Kurt Chowanski (MRS), Todd Ackerman(MRS), Jen Kelley, Hollings Scholarship Program.

LITERATURE CITED

Anderson, E., Z. Bai, C. Bischof, S. Blackford, J. Demmel, J. Dongarra, J. Du Croz, A. Greenbaum, S. Hammarling, A. McKenney, and D. Sorensen. 1999. LAPACK User's Guide, (http://www.netlib.org/lapack/lug/lapack_lug.html), Third Edition, SIAM, Philadelphia.

Anquetin, S., C. Guilbaud, and J. Chollet. 1998. The formation and destruction of inversion layers within a deep valley, J. Applied Met., *37*, 1547-1560.

Barr, S. and M. M. Orgill. 1989. Influence of external meteorology on nocturnal valley drainage winds, J. Applied Met., *28*, 497-517.

Gallant, J.C. and T. I. Dowling. 2003. A multiresolution index of valley bottom flatness for mapping depositional areas. Water Resour. Res., 39:1347, doi:10.10129/2002WR001426,2003.

Hamlet, A. F., P. W. Mote, M. P. Clark, D. P. Lettenmaier. 2005. Effects of temperature and precipitation variability on snowpack trends in the western U.S., J. Clim., 18:4545-4561.

Hubbart, J., T. Link, C. Campbell, and D. Cobos. 2005. Evaluation of a low-cost temperature measurement system for environmental applications. Hydrol. Process. 19:1517–1523.

Kalnay, E., and Coauthors. 1996. The NCEP/NCAR 40-Year Reanalysis Project, Bull. Amer. Meteor. Soc., 77:437-471.

Liston, G. E, and K. Elder. 2006. A meteorological distribution system for high-resolution terrestrial modeling (MicroMet), J. Hydromet., 7:217-234.

Lundquist, J.D., D.R. Cayan and M.D. Dettinger. 2003. Meteorology and hydrology in Yosemite National Park: A sensor network application. In Information Processing in Sensor Networks, F. Zhao and L. Guibas (eds.): IPSN 2003, LNCS 2634, 518-528.

Lundquist, J., D. Cayan, and M. Dettinger. 2004. Spring onset in the Sierra Nevada: When is snowmelt independent of elevation? J. Hydromet., 5:325-340.

Lundquist, J.D. and D. R. Cayan. 2007. Surface temperature patterns in complex terrain: daily variations and long-term change in the central Sierra Nevada, California. J. Geophys. Res., in press.

McGurk B. J., T. J. Edens, and D. L. Azuma. 1993. Predicting wilderness snow water equivalent with nonwilderness snow sensors. Water Resour. Bull., 29:85-94.

Neff, W. D. and C. W. King. 1989. The accumulation and pooling of drainage flows in a large basin, J. Applied Met., 28:518-529.

Preisendorfer, R. W. 1988. Principal Component Analysis in Meteorology and Oceanography. Number 17 in Developments in Atmospheric Science. Elsevier Science, Amsterdam.

Singh, P. 1991. A temperature lapse rate study in Western Himalayas. Hydrology, Jour. of Indian Assoc. of Hydrologists, 14:156-163.

Stewart, I. T., D. R. Cayan, and M. D. Dettinger. 2005. Changes towards earlier streamflow timing across Western North America, J. Climate, 18:1136-1155.